Three-cluster dynamics within an *ab initio* framework

Sofia Quaglioni,[1,*] Carolina Romero-Redondo,[2,†] and Petr Navrátil[2,‡]
[1]*Lawrence Livermore National Laboratory, P.O. Box 808, L-414, Livermore, California 94551, USA*
[2]*TRIUMF, 4004 Wesbrook Mall, Vancouver, British Columbia V6T 2A3, Canada*
(Received 1 August 2013; published 26 September 2013)

We introduce a fully antisymmetrized treatment of three-cluster dynamics within the *ab initio* framework of the no-core shell model/resonating-group method. Energy-independent nonlocal interactions among the three nuclear fragments are obtained from realistic nucleon-nucleon interactions and consistent *ab initio* many-body wave functions of the clusters. The three-cluster Schrödinger equation is solved with bound-state boundary conditions by means of the hyperspherical-harmonic method on a Lagrange mesh. We discuss the formalism in detail and give algebraic expressions for systems of two single nucleons plus a nucleus. Using a soft similarity-renormalization-group evolved chiral nucleon-nucleon potential, we apply the method to a $^4\mathrm{He} + n + n$ description of ^{6}He and compare the results to experiment and to a six-body diagonalization of the Hamiltonian performed within the harmonic-oscillator expansions of the no-core shell model. Differences between the two calculations provide a measure of core (^{4}He) polarization effects.

DOI: 10.1103/PhysRevC.88.034320 PACS number(s): 21.60.De, 25.10.+s, 27.20.+n

I. INTRODUCTION

In nuclear physics, *ab initio* approaches seek to solve the many-body Schrödinger equation in terms of constituent protons and neutrons interacting through nucleon-nucleon (NN) and three-nucleon ($3N$) forces that yield a high-precision fit of two- and three-body data. Their aim is twofold: first, to help unfold the true nature of the force among nucleons and, second, to arrive at a fundamental understanding of nuclei and their role in the universe.

In three- and four-nucleon systems, where a numerically exact solution of the quantum-mechanical problem for both negative [1] and positive energies [2] is now possible, this goal has been largely achieved. For heavier systems, *ab initio* calculations have been mostly confined to the description of the bound-state properties of stable nuclei but are now starting to be extended to dynamical processes between nuclei. The Green's function Monte Carlo method has been used to describe the elastic scattering of neutrons on ^{4}He [3] and to compute asymptotic normalization coefficients [4] and nuclear widths [5]. Loosely bound and unbound nuclear states have been addressed within the coupled-cluster technique [6,7] by using a Berggren basis and this method has recently been applied to compute elastic proton scattering on ^{40}Ca [8].

An *ab initio* framework that promises to provide a unified treatment of a wide range of nuclear phenomena (well-bound states, loosely bound and unbound exotic nuclei, scattering and reaction observables) is the no-core shell model with continuum (NCSMC) [9,10]. Here, the nuclear many-body states are seen as superimpositions of continuous $(A-a, a)$ binary-cluster wave functions in the spirit of the resonating-group method (RGM) [11–16] and square-integrable eigenstates of the A-nucleon system, in which each cluster of nucleons and the compound nuclear states are obtained within the *ab inito* no-core shell model (NCSM) [17,18]. So far, we have laid the foundations of the NCSMC by developing the formalism to compute nucleon-nucleus collisions and applying it to the description of the unbound ^{7}He nucleus. However, expansions on the NCSM/RGM portion of the basis [19,20] have already been successfully used to describe nucleon [21] and deuteron [22] scattering on light nuclei and achieve the first *ab initio* description of $^7\mathrm{Be}(p,\gamma)^8\mathrm{B}$ radiative capture [23] and $^3\mathrm{H}(d,n)^4\mathrm{He}$ and $^3\mathrm{He}(d,p)^4\mathrm{He}$ fusion rates [24], based on realistic NN interactions. Work is currently under way to incorporate the $3N$ force into this binary-reaction formalism and to attain the description of deuteron-nucleus scattering and transfer reactions within the NCSMC approach.

Achieving an *ab initio* treatment of three-cluster dynamics is another important stepping stone towards gaining a basic understanding of nuclei and their reactions. To cite a few instances, important nuclear fusion processes such as the $^3\mathrm{H}(^3\mathrm{H},2n)^4\mathrm{He}$ or $^3\mathrm{He}(^3\mathrm{He},2p)^4\mathrm{He}$ reactions are characterized by three-body final states. In addition, only with an approach capable of accounting for three-cluster configurations can one obtain an accurate description of Borromean nuclei, ternary systems of two nucleons orbiting around a tightly bound core whose components are not bound in pairs. Finally, three-body configurations can be necessary even at very low energy to achieve a proper treatment of polarization and virtual excitations of breakup channels in reactions with weakly bound projectiles such as the deuteron.

Microscopic three-cluster models, where all nucleons are taken into account and the Pauli principle is treated exactly, have been used for some time, particularly in combination with the hyperspherical formalism for the solution of the dynamic equations [25–30]. However, they have two main limitations: the use of central NN potentials with state-dependent parameters adjusted to reproduce the binding energy of the system under study, occasionally complemented with a spin-orbit interaction; and a simplified description of the internal structure of the clusters, which are in most cases described by s-shell wave functions. In this paper, we report on an extension of the

*quaglioni1@llnl.gov
†cromeroredondo@triumf.ca
‡navratil@triumf.ca

NCSM/RGM formalism to treat the dynamics among three nuclei made of fully antisymmetrized interacting nucleons. The solution of the three-cluster Schrödinger equation is obtained by means of hyperspherical harmonic (HH) expansions on a Lagrange mesh [31,32]. In addition, we present the first ^{4}He $+ n + n$ investigation of the ground state (g.s.) of the ^{6}He nucleus based on an NN potential that yields a high-precision fit of the NN phase shifts and *ab initio* four-body wave functions for the ^{4}He cluster obtained consistently from the same Hamiltonian. In particular, we employ a similarity-renormalization-group (SRG) [33,34] evolved chiral N^{3}LO NN [35] potential. For this first application, we include only the g.s. of the ^{4}He cluster and estimate the importance of the core polarization by comparing the results obtained with six-body NCSM diagonalizations of the adopted Hamiltonian. The inclusion of excited states of ^{4}He to describe such effects is hard and not very efficient within the NCSM/RGM approach. On the other hand, core-polarization effects will be easily accounted for once the present formalism is embedded within the NCSMC framework.

The paper is organized as follows. In Sec. II we define the microscopic three-cluster problem, present a brief overview of the HH functions and their application within the R-matrix method on Lagrange mesh for the solution of the three-body bound-state problem, and introduce in detail the three-cluster NCSM/RGM formalism. In particular, in Sec. II E we present algebraic expressions for systems of two single nucleons plus a nucleus. Results for the g.s. of the ^{6}He Borromean nucleus are presented in Sec. III, where we discuss calculations performed by solving the ^{4}He(g.s.) $+ n + n$ NCSM/RGM equations and compare them with a diagonalization of the Hamiltonian in the six-body NCSM model space. Conclusions and outlook are given in Sec. IV. Finally, additional details on the formalism are presented in the Appendixes.

II. FORMALISM

A. Microscopic three-cluster problem

The intrinsic motion of a system of A nucleons arranged into three clusters, of mass number $A - a_{23}$, a_2, and a_3 ($a_{23} = a_2 + a_3 < A$), respectively, can be described by the many-body wave function

$$|\Psi^{J^\pi T}\rangle = \sum_\nu \iint dx\, dy\, x^2\, y^2\, G_\nu^{J^\pi T}(x,y)\, \hat{\mathcal{A}}_\nu \left|\Phi_{\nu xy}^{J^\pi T}\right\rangle, \quad (1)$$

where $G_\nu^{J^\pi T}(x,y)$ are continuous variational amplitudes of the integration variables x and y, $\hat{\mathcal{A}}_\nu$ is an appropriate intercluster antisymmetrizer introduced to guarantee the exact preservation of the Pauli exclusion principle, and

$$\left|\Phi_{\nu xy}^{J^\pi T}\right\rangle = \left[\left(\left|A - a_{23}\alpha_1 I_1^{\pi_1} T_1\right\rangle\left(\left|a_2\,\alpha_2 I_2^{\pi_2} T_2\right\rangle\left|a_3\,\alpha_3 I_3^{\pi_3} T_3\right\rangle\right)^{(s_{23}T_{23})}\right)^{(ST)}\left(Y_{\ell_x}(\hat{\eta}_{23})Y_{\ell_y}(\hat{\eta}_{1,23})\right)^{(L)}\right]^{(J^\pi T)} \frac{\delta(x-\eta_{23})}{x\eta_{23}}\frac{\delta(y-\eta_{1,23})}{y\eta_{1,23}} \quad (2)$$

are three-body cluster channels of total angular momentum J, parity π, and isospin T. Here, $|A - a_{23}\alpha_1 I_1^{\pi_1} T_1\rangle$, $|a_2\,\alpha_2 I_2^{\pi_2} T_2\rangle$, and $|a_3\,\alpha_3 I_3^{\pi_3} T_3\rangle$ denote the microscopic (antisymmetric) wave functions of the three nuclear fragments, which are labeled by the spin-parity, isospin, and energy quantum numbers $I_i^{\pi_i}$, T_i, and α_i, respectively, with $i = 1, 2, 3$. Additional quantum numbers characterizing the basis states of Eq. (2) are the spins $\vec{s}_{23} = \vec{I}_2 + \vec{I}_3$ and $\vec{S} = \vec{I}_1 + \vec{s}_{23}$, the orbital angular momenta ℓ_x, ℓ_y, and $\vec{L} = \vec{\ell}_x + \vec{\ell}_y$, and the isospin $\vec{T}_{23} = \vec{T}_2 + \vec{T}_3$. In our notation, all these quantum numbers are grouped under the cumulative index $\nu = \{A - a_{23}\,\alpha_1 I_1^{\pi_1} T_1; a_2\,\alpha_2 I_2^{\pi_2} T_2;\ a_3\,\alpha_3 I_3^{\pi_3} T_3;\ s_{23}\,T_{23}\,S\,\ell_x\,\ell_y\,L\}$. Besides the translationally invariant coordinates (see, e.g., Ref. [20] Sec. II.C) used to describe the internal dynamics of clusters 1, 2, and 3, respectively, in Eq. (2) we have introduced the Jacobi coordinates $\vec{\eta}_{1,23}$ and $\vec{\eta}_{23}$, where

$$\vec{\eta}_{1,23} = \eta_{1,23}\hat{\eta}_{1,23} = \sqrt{\frac{a_{23}}{A(A-a_{23})}}\sum_{i=1}^{A-a_{23}}\vec{r}_i - \sqrt{\frac{A-a_{23}}{A\,a_{23}}}\sum_{j=A-a_{23}+1}^{A}\vec{r}_j \quad (3)$$

is the relative vector proportional to the displacement between the center of mass (c.m.) of the first cluster and that of the residual two fragments, and

$$\vec{\eta}_{23} = \eta_{23}\hat{\eta}_{23} = \sqrt{\frac{a_3}{a_{23}\,a_2}}\sum_{i=A-a_{23}+1}^{A-a_3}\vec{r}_i - \sqrt{\frac{a_2}{a_{23}\,a_3}}\sum_{j=A-a_3+1}^{A}\vec{r}_j \quad (4)$$

is the relative coordinate proportional to the distance between the center of mass of cluster 2 and that of cluster

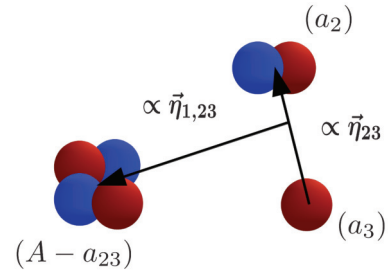

FIG. 1. (Color online) We show the Jacobi coordinates $\vec{\eta}_{1,23}$ (proportional to the vector between the c.m. of the first cluster and that of the residual two fragments) and $\vec{\eta}_{23}$ (proportional to the vector between the c.m. of cluster 2 and that of cluster 3). A case with three clusters, of four, two, and one nucleons, is shown, however, the formalism is completely general and can be used to describe any three-cluster configuration.

3 (see Fig. 1). Here, $\vec{r}_i$ denotes the position vector of the ith nucleon.

Using expansion (1) for the wave function and projecting the microscopic A-body Schrödinger equation onto the basis states $\hat{\mathcal{A}}_\nu\,|\Phi^{J^\pi T}_{\nu xy}\rangle$, the many-body problem can be mapped onto the system of coupled-channel integral-differential equations

$$\sum_\nu \iint dx\,dy\,x^2y^2\big[\mathcal{H}^{J^\pi T}_{\nu'\nu}(x',y',x,y) - E\,\mathcal{N}^{J^\pi T}_{\nu'\nu}(x',y',x,y)\big] \times G^{J^\pi T}_\nu(x,y) = 0 \tag{5}$$

for the unknown variational amplitudes $G^{J^\pi T}_\nu(x,y)$. Here, E is the total energy of the system in the c.m. frame and

$$\mathcal{H}^{J^\pi T}_{\nu'\nu}(x',y',x,y) = \big\langle \Phi^{J^\pi T}_{\nu' x' y'}\big|\hat{\mathcal{A}}_{\nu'} H \hat{\mathcal{A}}_\nu\big|\Phi^{J^\pi T}_{\nu xy}\big\rangle, \tag{6}$$

$$\mathcal{N}^{J^\pi T}_{\nu'\nu}(x',y',x,y) = \big\langle \Phi^{J^\pi T}_{\nu' x' y'}\big|\hat{\mathcal{A}}_{\nu'} \hat{\mathcal{A}}_\nu\big|\Phi^{J^\pi T}_{\nu xy}\big\rangle \tag{7}$$

are integration kernels given, respectively, by the Hamiltonian and overlap (or norm) matrix elements over the antisymmetrized basis states of Eq. (2). Finally, H is the intrinsic A-body Hamiltonian. Denoting by $\bar{V}_C$ the sum of the pairwise average Coulomb interactions among the three clusters in channel ν of charge numbers $Z_{\nu 1}$, $Z_{\nu 2}$, and $Z_{\nu 3}$, this can be separated into relative-motion and clusters' intrinsic Hamiltonians according to

$$H = T_{\rm rel} + \bar{V}_C + \mathcal{V}_{\rm rel} + H_{(A-a_{23})} + H_{(a_2)} + H_{(a_3)}\,, \tag{8}$$

with $T_{\rm rel}$ the relative kinetic energy operator for the three-body system and $\mathcal{V}_{\rm rel}$ the intercluster potential given by

$$\mathcal{V}_{\rm rel} = \sum_{i=1}^{A-a_{23}} \sum_{j=A-a_{23}+1}^{A} V_{ij} + \sum_{k=A-a_{23}+1}^{A-a_3} \sum_{l=A-a_3+1}^{A} V_{kl} + \mathcal{V}^{3N}_{(A-a_{23},a_2,a_3)} - \bar{V}_C\,. \tag{9}$$

Here, $\mathcal{V}^{3N}_{(A-a_{23},a_2,a_3)}$ encompasses the portion of intercluster interactions owing to the $3N$ force, which, in general, is part of a realistic Hamiltonian, and V_{ij} is the (nuclear plus point–Coulomb) interaction between nucleon i and nucleon j. In the present paper we consider only the NN component of the intercluster interaction and disregard, for the time being, the term $\mathcal{V}^{3N}_{(A-a_{23},a_2,a_3)}$. Inclusion of the $3N$ force into the formalism, although computationally much more involved, is straightforward and will be the matter of future investigations. In the remainder of the paper, we also omit the average Coulomb potential $\bar{V}_C$, which is null for neutral systems such as the ^{4}He $+\,n\,+\,n$ investigated here. The treatment of charged systems is, nevertheless, possible and can be implemented along the same lines as in Ref. [32].

B. Orthogonalized equations

Owing to the presence of the norm kernel, the three-cluster equations (5) contain energy-dependent coupling terms. Alternatively, one can introduce the orthogonalized Hamiltonian kernel $\bar{\mathcal{H}}^{J^\pi T}_{\nu'\nu}(x',y',x,y)$ of Eq. (A1) and solve the more familiar system of multichannel Schrödinger equations

$$\sum_\nu \iint dx\,dy\,x^2y^2\Big[\bar{\mathcal{H}}^{J^\pi T}_{\nu'\nu}(x',y',x,y) - E\,\delta_{\nu\nu'}\frac{\delta(x'-x)}{x'x}\frac{\delta(y'-y)}{y'y}\Big]\chi^{J^\pi T}_\nu(x,y) = 0. \tag{10}$$

The amplitudes $G^{J^\pi T}_\nu(x,y)$ of Eq. (1) can then be recovered from the Schrödinger wave functions $\chi^{J^\pi T}_\nu(x,y)$ through Eq. (A2). More details on the orthogonalization procedure are given in Appendix A.

C. Hyperspherical harmonics

The three-cluster Schrödinger equations, (10), can be conveniently solved within the HH basis. This basis is broadly used [36] to treat few-body problems, as its elements are eigenfunctions of the angular part of the kinetic operator written in hyperspherical coordinates [37]. The first step is to move to hyperspherical coordinates, i.e.,

$$\eta_{23} = \rho_\eta \sin\alpha_\eta, \quad x = \rho\sin\alpha, \tag{11}$$

$$\eta_{1,23} = \rho_\eta \cos\alpha_\eta, \quad y = \rho\cos\alpha, \tag{12}$$

where ρ_η and ρ are hyper-radii, and α_η and α hyperangles. In these coordinates, the relative kinetic energy operator for the three-cluster system can be written as

$$\hat{T}_{\rm rel} = -\frac{\hbar^2}{2m}\left(\frac{\partial^2}{\partial\rho^2} + \frac{5}{\rho}\frac{\partial}{\partial\rho} - \frac{\hat{\Lambda}^2}{\rho^2}\right), \tag{13}$$

where $\hat{\Lambda}^2$ is the grand-angular kinetic operator and m is the mass of the nucleon.

As anticipated, the elements of the HH basis are the eigenfunctions of $\hat{\Lambda}^2$

$$\mathcal{Y}^{K\ell_x\ell_y}_{LM_L}(\Omega) = \phi^{\ell_x,\ell_y}_K(\alpha)\big(Y_{\ell_x}(\hat{x})\,Y_{\ell_y}(\hat{y})\big)^{(L)}_{M_L}\,, \tag{14}$$

with eigenvalues $K(K+4)$. Here, K is the hypermomentum quantum number defined as $K = 2n + \ell_x + \ell_y$ with $n = 0, 1, 2, \ldots$, the notation Ω represents the hyperangle α and the four angles $\hat{x}$ and $\hat{y}$ (the direction angles of the Jacobi coordinates $\vec{x}$ and $\vec{y}$, respectively), and the complete set of functions $\phi^{\ell_x,\ell_y}_K(\alpha)$ is given by

$$\phi^{\ell_x,\ell_y}_K(\alpha) = N^{\ell_x\ell_y}_K(\sin\alpha)^{\ell_x}(\cos\alpha)^{\ell_y} P^{\ell_x+\frac{1}{2},\ell_y+\frac{1}{2}}_n(\cos 2\alpha), \tag{15}$$

where $P^{\alpha,\beta}_n(\xi)$ are Jacobi polynomials, and $N^{\ell_x\ell_y}_K$ normalization constants.

As shown in Appendix B, the HH functions, (14), form a natural basis for the description of the three-cluster wave function of Eq. (1) and for the solution of the three-cluster dynamical equations. Indeed, by (i) using the expansion

$$\chi^{J^\pi T}_\nu(\rho,\alpha) = \frac{1}{\rho^{5/2}}\sum_K u^{J^\pi T}_{K\nu}(\rho)\phi^{\ell_x,\ell_y}_K(\alpha) \tag{16}$$

for the relative motion wave functions, where $u^{J^\pi T}_{K\nu}(\rho)$ are hyper-radial functions analogous to those of Eq. (B6), and

(ii) projecting from the left on the basis states $\phi^{\ell'_x,\ell'_y}_{K'}(\alpha')$, Eq. (10) can be written as a set of nonlocal integral-differential equations in the hyper-radial coordinates:

$$\sum_{K\nu}\int d\rho\rho^5 \bar{\mathcal{H}}^{K'K}_{\nu'\nu}(\rho',\rho)\frac{u^{J^\pi T}_{K\nu}(\rho)}{\rho^{5/2}} = E\frac{u^{J^\pi T}_{K'\nu'}(\rho')}{\rho'^{5/2}}. \quad (17)$$

Here, the orthogonalized Hamiltonian kernel in the hyper-radial variables ρ and ρ' is given by

$$\bar{\mathcal{H}}^{K'K}_{\nu'\nu}(\rho',\rho) = \int d\alpha' \sin^2\alpha' \cos^2\alpha' \int d\alpha \sin^2\alpha\cos^2\alpha \times \phi^{\ell'_x,\ell'_y}_{K'}(\alpha')\,\bar{\mathcal{H}}^{J^\pi T}_{\nu'\nu}(\rho',\alpha',\rho,\alpha)\,\phi^{\ell_x,\ell_y}_{K}(\alpha). \quad (18)$$

The solution of Eq. (17) for the case in which the three clusters form a bound state can be conveniently achieved within the R-matrix method as discussed in the next section.

D. Solution of the three-cluster equations for bound states

We calculate the relative motion wave function by solving Eq. (17) with the calculable R-matrix method [38]. In particular, we use a Lagrange mesh which simplifies the problem as shown in many previous works for the two-cluster case [39–42] and was generalized to the three-cluster problem in Ref. [31]. Within this method, the configuration space is divided into two regions by assuming that the Coulomb interaction (if present) is the only interaction experienced by the clusters beyond a finite separation $\rho = a$.

In the external region ($\rho > a$), where the Schrödinger equation can be solved exactly, the hyper-radial wave function is approximated by its known asymptotic form for large ρ. For bound states of neutral systems (such as the one investigated in this paper), such an asymptotic solution is given by

$$u^{J^\pi T}_{K\nu,\mathrm{ext}}(\rho) = B_{K\nu}\sqrt{k\rho}\,K_{K+2}(k\rho), \quad (19)$$

where $K_{K+2}(k\rho)$ is a modified Bessel function of the second kind, $k^2 = -2mE/\hbar^2$ is the wave number, and $B_{K\nu}$ is a constant. In the internal region ($\rho \leqslant a$), where also the mutual nuclear interaction among the clusters is present, the wave function is written as a variational expansion on a Lagrange basis of N functions $f_i(\rho)$ (see Appendix C for definition),

$$u^{J^\pi T}_{K\nu,\mathrm{int}}(\rho) = \sum_{i=1}^{N}\beta_{K\nu i}\,f_i(\rho), \quad (20)$$

where $\beta_{K\nu i}$ are the coefficients of the expansion. The radial wave functions are then obtained by solving in the internal region the set of Bloch-Schrödinger equations

$$\sum_{K\nu}\int d\rho\rho^5\left[\bar{\mathcal{H}}^{K'K}_{\nu'\nu}(\rho',\rho) + (\mathcal{L}_{K\nu}(\rho) - E)\frac{\delta(\rho-\rho')}{\rho^5}\delta_{\nu'\nu}\delta_{K'K}\right]\frac{u^{J^\pi T}_{K\nu,\mathrm{int}}(\rho)}{\rho^{5/2}} = \mathcal{L}_{K'\nu'}(\rho')\frac{u^{J^\pi T}_{K'\nu',\mathrm{ext}}(\rho')}{\rho'^{5/2}}, \quad (21)$$

supplemented by the continuity condition $u^{J^\pi T}_{K\nu,\mathrm{int}}(a) = u^{J^\pi T}_{K\nu,\mathrm{ext}}(a)$. Here, we have used the asymptotic expression of Eq. (19) on the right-hand side and the expansion of Eq. (20) on the left-hand side of the equation, respectively. Further, the elements of the Bloch operator ($L_{K\nu}$ being arbitrary constants) [32]

$$\mathcal{L}_{K\nu}(\rho) = \frac{\hbar^2}{2m}\delta(\rho-a)\frac{1}{\rho^{5/2}}\left(\frac{\partial}{\partial\rho} - \frac{L_{K\nu}}{\rho}\right)\rho^{5/2} \quad (22)$$

have the dual function of restoring the Hermiticity of the Hamiltonian in the internal region and enforcing the continuity of the derivative of the wave function at $\rho = a$ [38]. Owing to the Dirac's δ in the Bloch operator, the system of nonlocal equations (21) is equivalent to that of Eq. (17) in the internal region. Projecting Eq. (21) over a basis element $f_{i'}(\rho')$ and choosing the logarithmic derivative evaluated in a

$$L_{K\nu}(E) = a\frac{u'^{J^\pi T}_{K\nu,\mathrm{ext}}(a)}{u^{J^\pi T}_{K\nu,\mathrm{ext}}(a)} \quad (23)$$

for the constants appearing in the definition of the Bloch operator, (22), system (21) reduces to

$$\sum_{K'\nu'i'}\left[C^{J^\pi T}_{K\nu i,K'\nu'i'} - E\delta_{\nu'\nu}\delta_{K'K}\delta_{i'i}\right]\beta_{K'\nu'i'} = 0, \quad (24)$$

where the elements of the matrix $C^{J^\pi T}$ are given by the integrals over the internal region,

$$C^{J^\pi T}_{K'\nu'i',K\nu i} = \int_0^a d\rho'\int_0^a d\rho\rho^5 f_{i'}(\rho') \times\left(\bar{\mathcal{H}}^{K'K}_{\nu'\nu}(\rho',\rho) + \mathcal{L}_{K\nu}\delta_{\nu'\nu}\delta_{K'K}\frac{\delta(\rho'-\rho)}{\rho^5}\right)f_i(\rho). \quad (25)$$

The choice of Lagrange functions as square-integrable basis states for the expansion of the wave function in the internal region of Eq. (20) greatly simplifies the evaluation of these integrals. Indeed, within the Gauss quadrature approximation, the Lagrange functions are orthogonal to each other (see Appendix C), the matrix elements of nonlocal potentials are proportional to the values of the nonlocal potentials at the mesh points, and the analytical expression for the matrix elements of the kinetic energy operator is straightforward to obtain.

Note that the matrix $C^{J^\pi T}$ depends on the energy, owing to the choice (23) of the boundary conditions in the Bloch operator, which are functions of the wave number k [see Eq. (19)]. In practice, the solution of Eq. (24) is obtained recursively. One can start from $L_{K\nu} = 0$ and iterate the solution of the eigenvalue equation, (24), until the convergence in E is reached, which typically occurs in a few iterations. The coefficients $\beta_{K\nu i}$ of the expansion (20) are then obtained from the corresponding eigenvector and the relative motion wave functions can be constructed using Eqs. (16) and (20).

E. Integration kernels

The norm and Hamiltonian integration kernels presented in Sec. II A are calculated within the NCSM/RGM approach as follows. First, the clusters' eigenstates appearing in Eq. (2) are obtained by diagonalizing the $H_{(A-a_{23})}$, $H_{(a_2)}$, and $H_{(a_3)}$

intrinsic Hamiltonians within the model spaces spanned by the $(A-a_{23})$-, a_2-, and a_3-nucleon NCSM bases, respectively. These are complete sets of many-body HO basis states, the size of which is defined by the maximum number $N_{\max}$ of HO quanta above the lowest configuration shared by the nucleons. The same HO frequency $\hbar\Omega$ is used for all three clusters, and the model-space size $N_{\max}$ is identical (differs by one) for states of the same (opposite) parity.

Second, for those components that are localized, the matrix elements of the translational invariant operators $\hat{\mathcal{A}}_{\nu'}\hat{\mathcal{A}}_{\nu}$, $\hat{\mathcal{A}}_{\nu'}H\hat{\mathcal{A}}_{\nu}$ entering the expression of the integration kernels are evaluated within an HO model space using the expansion

$$\begin{aligned}\left|\Phi^{J^\pi T}_{\nu xy}\right\rangle = \sum_{n_x n_y}\sum_{Z J_{23}} &\hat{Z}\hat{J}_{23}\hat{S}\hat{L}\,(-1)^{I_1+J_{23}+J+S+Z+\ell_x+\ell_y} \\ &\times \begin{Bmatrix} I_1 & s_{23} & S \\ \ell_x & Z & J_{23}\end{Bmatrix}\begin{Bmatrix} S & \ell_x & Z \\ \ell_y & J & L\end{Bmatrix} \\ &\times R_{n_x\ell_x}(x)R_{n_y\ell_y}(y)\left|\Phi^{J^\pi T}_{\gamma n_x n_y}\right\rangle, \end{aligned} \tag{26}$$

where $\hat{Z}=\sqrt{2Z+1}$, $\hat{J}_{23}=\sqrt{2J_{23}+1},\ldots,$ etc., and $|\Phi^{J^\pi T}_{\gamma n_x n_y}\rangle$ are the HO channel states defined by

$$\left|\Phi^{J^\pi T}_{\gamma n_x n_y}\right\rangle = \left[\left(\left|A-a_{23}\alpha_1 I_1^{\pi_1} T_1\right\rangle\left(Y_{\ell_x}(\hat{\eta}_{23})\left(\left|a_2\alpha_2 I_2^{\pi_2} T_2\right\rangle\left|a_3\alpha_3 I_3^{\pi_3} T_3\right\rangle\right)^{(s_{23}T_{23})}\right)^{(J_{23}T_{23})}\right)^{(ZT)} Y_{\ell_y}(\hat{\eta}_{1,23})\right]^{(J^\pi T)} R_{n_x\ell_x}(\eta_{23})R_{n_y\ell_y}(\eta_{1,23}) \tag{27}$$

and labeled by the channel index $\gamma=\{A-a_{23}\,\alpha_1 I_1^{\pi_1} T_1;\ a_2\,\alpha_2 I_2^{\pi_2} T_2;\ a_3\,\alpha_3 I_3^{\pi_3} T_3;\ell_x\ s_{23} J_{23}\ T_{23}\ Z\ \ell_y\}$. Besides the representation of the Dirac's δ functions of Eq. (2) in terms of HO radial wave functions $R_{n_x\ell_x}(x)$ and $R_{n_y\ell_y}(y)$, the transformation of Eq. (26) reflects a different coupling scheme of the HO channels, (27), with respect to the original basis, with J_{23} the total (orbital plus spin) angular momentum quantum number of the system formed by the second and third clusters and $\vec{Z}=\vec{I}_1+\vec{J}_{23}$ the new channel spin. While the configuration of Eq. (2) is dictated by the use of the HH as the basis for the solution of the three-cluster problem (see Sec. II C and Appendix B), the binary-cluster-like coupling scheme of Eq. (27) is more convenient for the derivation of the kernels in the HO basis, as will become clear in a moment. The frequency $\hbar\Omega$ and the model-space size ($N_{\max}/N_{\max}+1$ for even/odd parity states) used to expand the relative motion are the same as those adopted for the calculation of the clusters' eigenstates.

Finally, although the integration kernels are translational invariant quantities, it is computationally convenient to work within a Slater determinant (SD) channel basis $|\Phi^{J^\pi T}_{\gamma n_x n_y}\rangle_{\rm SD}$ defined as in Eq. (27) but with $\vec{R}^{(a_{23})}_{\rm c.m.}$ in place of the relative vector $\vec{\eta}_{1,23}$ and the eigenstates of the heaviest cluster obtained in the SD basis, i.e.,

$$\begin{aligned}\left|A-a_{23}\alpha_1 I_1^{\pi_1} T_1\right\rangle_{\rm SD} = &\left|A-a_{23}\alpha_1 I_1^{\pi_1} T_1\right\rangle R_{00}\left(R^{(A-a_{23})}_{\rm c.m.}\right) \\ &\times Y_{00}\left(\hat{R}^{(A-a_{23})}_{\rm c.m.}\right),\end{aligned} \tag{28}$$

where $\vec{R}^{(A-a_{23})}_{\rm c.m.}$ and $\vec{R}^{(a_{23})}_{\rm c.m.}$ are, respectively, the coordinates proportional to the c.m. of the first and last two clusters:

$$\vec{R}^{(A-a_{23})}_{\rm c.m.} = \frac{1}{\sqrt{A-a_{23}}}\sum_{i=1}^{A-a_{23}}\vec{r}_i, \tag{29}$$

$$\vec{R}^{(a_{23})}_{\rm c.m.} = \frac{1}{\sqrt{a_{23}}}\sum_{j=A-a_{23}+1}^{A}\vec{r}_j\,. \tag{30}$$

Indeed, the translational invariant matrix elements can be extracted from those calculated in the SD basis, which contain the spurious motion of the c.m., by inverting the following linear transformation:

$$\begin{aligned}{}_{\rm SD}\left\langle\Phi^{J^\pi T}_{\gamma' n'_x n'_y}\right|\hat{\mathcal{O}}_{\rm t.i.}\left|\Phi^{J^\pi T}_{\gamma n_x n_y}\right\rangle_{\rm SD} &= \sum_{n^{r\prime}_y\ell^{r\prime}_y, n^r_y\ell^r_y, J_r}\left\langle\Phi^{J^{\pi_r} T}_{\gamma_r' n'_x n^{r\prime}_y}\right|\hat{\mathcal{O}}_{\rm t.i.}\left|\Phi^{J^{\pi_r} T}_{\gamma_r n_x n^r_y}\right\rangle \\ &\times\sum_{\mathcal{NL}}\hat{\ell}_y\hat{\ell}'_y\hat{J}_r^2\,(-1)^{Z+\ell_y-Z'-\ell'_y} \\ &\times\begin{Bmatrix} Z & \ell^r_y & J_r \\ \mathcal{L} & J & \ell_y\end{Bmatrix}\begin{Bmatrix} Z' & \ell^{r\prime}_y & J_r \\ \mathcal{L} & J & \ell'_y\end{Bmatrix} \\ &\times\left\langle n^r_y\ell^r_y\,\mathcal{NL}\,\ell_y|00\,n_y\ell_y\,\ell_y\right\rangle_{\frac{a_{23}}{A-a_{23}}} \\ &\times\left\langle n^{r\prime}_y\ell^{r\prime}_y\,\mathcal{NL}\,\ell'_y|00\,n'_y\ell'_y\,\ell'_y\right\rangle_{\frac{a'_{23}}{A-a'_{23}}}.\end{aligned} \tag{31}$$

Here, γ_r denotes a channel index identical to γ except for the replacement of the quantum number ℓ_y with ℓ^r_y (the same applies for the primed indexes), $\pi_r=\pi(-1)^{\ell^r_y-\ell_y}=\pi_1\pi_2\pi_3(-1)^{\ell_x+\ell^r_y}$, and $\hat{\mathcal{O}}_{\rm t.i.}$ is any scalar and parity-conserving translational invariant operator. Further, the transformation of Eq. (31) is diagonal in all quantum numbers but n_y, ℓ_y, n'_y, ℓ'_y, and J^π. Although formally not strictly necessary, with the new angular momentum coupling scheme of Eq. (27), the present conversion from SD to translational invariant matrix elements represents a straightforward generalization of the analogous binary-cluster transformation discussed in Sec. II C 2 of Ref. [20] and the most advantageous choice from a computational point of view.

1. The (A-2,1,1) mass partition

The theoretical framework presented so far is general and can, in principle, be applied to any three-cluster system. In the following, we discuss the derivation of the integration kernels for the more specialized instance of a target nucleus plus two single nucleons (a_2, $a_3=1$), such as the ^{4}He $+\,n+n$ system investigated here. Specifically, we consider the case of

identical $(A-2,1,1)$ mass partitions in both the initial and the final states.

In this case, the second and third clusters are point-like nucleons with quantum numbers $I^{\pi_{2(3)}}_{2(3)} T_{2(3)} = \frac{1}{2}^+ \frac{1}{2}$, and the intercluster antisymmetrizer is simply given by the product of the antisymmetrization operators for an $(A-2,2)$ mass partition and that of a two-body system,

$$\begin{aligned}\hat{\mathcal{A}}_v &= \hat{\mathcal{A}}_{(A-2,2)} \frac{1}{\sqrt{2}}(1-\hat{P}_{A-1\,A}) \\ &= \sqrt{\frac{2}{(A-1)A}}\left[1-\sum_{i=1}^{A-2}(\hat{P}_{i\,A-1}+\hat{P}_{i\,A})+\sum_{i<j=1}^{A-2}\hat{P}_{i\,A-1}\hat{P}_{j\,A}\right] \\ &\quad\times\frac{1}{\sqrt{2}}(1-\hat{P}_{A-1\,A}). \end{aligned} \tag{32}$$

Although other factorizations of this operator are of course possible, with the present choice the antisymmetrization of nucleons $A-1$ and A is trivial and can be included in the definition of the channel basis; i.e.,

$$\left|\tilde{\Phi}^{J^\pi T}_{\nu xy}\right\rangle = \frac{1-(-1)^{\ell_x+s_{23}+T_{23}}}{\sqrt{2}}\left|\Phi^{J^\pi T}_{\nu xy}\right\rangle. \tag{33}$$

The integration kernels for the $(A-2,1,1)$ mass partition are then obtained by evaluating the matrix elements of the operators $\hat{\mathcal{A}}^2_{(A-2,2)} = \sqrt{(A-1)A/2}\,\hat{\mathcal{A}}_{(A-2,2)}$ and $\hat{\mathcal{A}}_{(A-2,2)} H \hat{\mathcal{A}}_{(A-2,2)} = \frac{1}{2}(\hat{\mathcal{A}}^2_{(A-2,2)} H + H \hat{\mathcal{A}}^2_{(A-2,2)})$ on the basis of Eq. (33). For the norm kernel of Eq. (7), this yields the following sum of a direct and an exchange term:

$$\begin{aligned}\mathcal{N}^{J^\pi T}_{\nu'\nu}(x',y',x,y) &= (1-(-1)^{\ell_x+s_{23}+T_{23}})\delta_{\nu'\nu} \\ &\quad\times\frac{\delta(x'-x)}{x'x}\frac{\delta(y'-y)}{y'y} \\ &\quad+\mathcal{N}^{\rm ex}_{\nu'\nu}(x',y',x,y). \end{aligned} \tag{34}$$

Here, the direct term arising from the identical permutation in the antisymmetrization operator is calculated in the full space, whereas the nonlocal exchange term is evaluated within the HO model space. As explained in the previous section, this is achieved by using expansion (26), with the translational invariant matrix elements on the HO channel basis of Eq. (27) (antisymmetrized for the exchange of nucleons $A-1$ and A),

$$\begin{aligned}&\mathcal{N}^{\rm ex}_{\gamma' n'_x n'_y,\gamma n_x n_y} \\ &\quad= -2(A-2)\left\langle\tilde{\Phi}^{J^\pi T}_{\gamma' n'_x n'_y}\middle|\hat{P}_{A-2\,A}\middle|\tilde{\Phi}^{J^\pi T}_{\gamma n_x n_y}\right\rangle \\ &\qquad+\frac{(A-2)(A-3)}{2}\left\langle\tilde{\Phi}^{J^\pi T}_{\gamma' n'_x n'_y}\middle|\hat{P}_{A-2\,A}\hat{P}_{A-3\,A-1}\middle|\tilde{\Phi}^{J^\pi T}_{\gamma n_x n_y}\right\rangle, \end{aligned} \tag{35}$$

obtained from the corresponding SD ones by inverting Eq. (31). At the same time, calculation of the matrix elements over the SD channels $|\tilde{\Phi}^{J^\pi T}_{\gamma n_x n_y}\rangle_{\rm SD}$ of Eq. (27) is achieved by first performing a transformation to a fully single-particle basis; i.e.,

$$\begin{aligned}\left|\tilde{\Phi}^{J^\pi T}_{\gamma n_x n_y}\right\rangle_{\rm SD} &= \sum_{abIL}\hat{Z}\hat{I}\hat{J}_{23}\hat{s}_{23}\hat{j}_a\hat{j}_b\hat{L}^2(-1)^{I_1+J+\ell_x+\ell_y+T_{23}} \\ &\quad\times\langle n_a\ell_a\, n_b\ell_b\, L|n_y\ell_y\, n_x\ell_x\, L\rangle_{d=1} \\ &\quad\times\begin{Bmatrix} I_1 & J_{23} & Z \\ \ell_y & J & I\end{Bmatrix}\begin{Bmatrix}\ell_y & L & \ell_x \\ s_{23} & J_{23} & I\end{Bmatrix} \\ &\quad\times\begin{Bmatrix}\ell_a & \ell_b & L \\ \frac{1}{2} & \frac{1}{2} & s_{23} \\ j_a & j_b & I\end{Bmatrix}\left|\Phi^{J^\pi T}_{\kappa_{ab}}\right\rangle_{\rm SD}. \end{aligned} \tag{36}$$

Here, a and b stand for the collections of HO single-particle quantum numbers $\{n_a\ell_a j_a\}$ and $\{n_b\ell_b j_b\}$, respectively; $\langle n_a\ell_a\, n_b\ell_b\, L|n_y\ell_y\, n_x\ell_x\, L\rangle_{d=1}$ indicates an HO bracket for two particles of equal mass; and $\kappa_{ab} = \{A-2\,\alpha_1 I^{\pi_1}_1 T_1; n_a\ell_a j_a \tfrac{1}{2}; n_b\ell_b j_b \tfrac{1}{2}; I T_{23}\}$ is the index labeling the new SD channel basis,

$$\begin{aligned}\left|\Phi^{J^\pi T}_{\kappa_{ab}}\right\rangle_{\rm SD} &= \Big[|A-2\,\alpha_1 I_1 T_1\rangle_{\rm SD}\big(\varphi_{n_a\ell_a j_a\frac{1}{2}}(\vec{r}_A\sigma_A\tau_A) \\ &\quad\times\varphi_{n_b\ell_b j_b\frac{1}{2}}(\vec{r}_{A-1}\sigma_{A-1}\tau_{A-1})\big)^{(IT_{23})}\Big]^{(J^\pi T)}. \end{aligned} \tag{37}$$

We note that, except for a difference in the notation used for the total isospin of nucleons $A-1$ and A, this basis is identical to that introduced for the treatment of binary-cluster channels with a dinucleon projectile in Eq. (18) of Ref. [22], where the interested reader can also find the algebraic expressions of the matrix elements ${}_{\rm SD}\langle\Phi^{J^\pi T}_{\kappa'_{ab}}|\hat{P}_{A-2\,A}|\Phi^{J^\pi T}_{\kappa_{ab}}\rangle_{\rm SD}$ and ${}_{\rm SD}\langle\Phi^{J^\pi T}_{\kappa'_{ab}}|\hat{P}_{A-2\,A}\hat{P}_{A-3\,A-1}|\Phi^{J^\pi T}_{\kappa_{ab}}\rangle_{\rm SD}$ in Eqs. (19) and (20), respectively.

The calculation of the Hamiltonian kernel of Eq. (6) is achieved along the same lines. In this case, the kernel can be divided into a term proportional to the norm kernel discussed above, plus a term which resembles the expression of the potential kernel for binary-cluster channels with a dinucleon projectile (see Ref. [22], Sec. II B),

$$\begin{aligned}&\left\langle\tilde{\Phi}^{J^\pi T}_{\nu' x' y'}\middle|H\hat{\mathcal{A}}^2_{(A-2,2)}\middle|\tilde{\Phi}^{J^\pi T}_{\nu xy}\right\rangle \\ &\quad=\left[\hat{T}_{\rm rel}+\hat{V}(x')+E^{I'_1T'_1}_{\alpha'}\right]\mathcal{N}^{J^\pi T}_{\nu'\nu}(x',y',x,y) \\ &\qquad+\left\langle\tilde{\Phi}^{J^\pi T}_{\nu' x' y'}\middle|\mathcal{V}^{(A-2,2)}_{\rm rel}\hat{\mathcal{A}}^2_{(A-2,2)}\middle|\tilde{\Phi}^{J^\pi T}_{\nu xy}\right\rangle, \end{aligned} \tag{38}$$

with an analogous expression for the matrix elements of the Hermitian conjugate operator $\hat{\mathcal{A}}^2_{(A-2,2)}H$. Here, $\hat{T}_{\rm rel}$ acts on the x' and y' coordinates, $\hat{V}(x')$ is the potential between nucleon A and nucleon $A-1$, $E^{I'_1T'_1}_{\alpha'}$ is the energy of the $(A-2)$-nucleon eigenstate in the final channel, and $\mathcal{V}^{(A-2,2)}_{\rm rel}$ is the sum of pairwise interactions corresponding to the first term on the right-hand side of Eq. (9).

As for the exchange operators of the norm, the matrix elements of $\mathcal{V}^{(A-2,2)}_{\rm rel}\hat{\mathcal{A}}^2_{(A-2,2)}$ are calculated within the HO model space. This involves the evaluation, on the SD channel basis of Eq. (37), of five potential terms: (i) $V_{A-2\,A-1}(1-\hat{P}_{A-2\,A-1})$, (ii) $V_{A-2\,A}\hat{P}_{A-2\,A-1}$, (iii) $V_{A-3\,A}(1-\hat{P}_{A-3\,A})\hat{P}_{A-2\,A-1}$, (iv) $V_{A-3\,A-1}\hat{P}_{A-2\,A-1}$, and (v) $V_{A\,A-4}(1-\hat{P}_{A-2\,A-1})\hat{P}_{A-3\,A}$. Algebraic expressions for these matrix elements can be found in Eqs. (A1)–(A4) and (24) in Ref. [22].

Differently from the deuteron-nucleus formalism in Ref. [22], where this interaction is already taken into account in the calculation of the (bound) projectile eigenstate, here the Hamiltonian kernel contains the additional contribution coming from the action of the operator $\hat{V}(x')$ on the norm kernel. In the absence of Coulomb interaction between the last two nucleons (which, if present, can be treated separately as explained in Sec. II A), this term is localized in the variables x', x and can be calculated as

$$\begin{aligned}
&\hat{V}(x')\mathcal{N}^{J^\pi T}_{\nu'\nu}(x',y',x,y)\\
&\quad=\hat{S}\hat{S}'\hat{L}\hat{L}'(-1)^{\ell_x+S+L-\ell'_x-S'-L'}\\
&\qquad\times\sum_{J_{23}}\hat{J}^2_{23}\begin{Bmatrix}- & I_1 & S' & s_{23}\\ \ell_y & - & L' & \ell'_x\\ \ell_x & s_{23} & - & J_{23}\\ L & S & J & -\end{Bmatrix}\\
&\qquad\times\sum_{L_x}\sum_{n'_x n_x}R_{n'_x\ell'_x}(x')R_{n_xL_x}(x)\\
&\qquad\times\langle n'_x\ell'_x s_{23}J_{23}T_{23}|V|n_xL_xs_{23}J_{23}T_{23}\rangle\\
&\qquad\times(1-(-1)^{\ell_x+s_{23}+T_{23}})\delta_{\tilde{\gamma}'\gamma}\frac{\delta(y'-y)}{y'y}\\
&\qquad+\hat{V}(x')\mathcal{N}^{\rm ex}_{\nu'\nu}(x',y',x,y).
\end{aligned}\tag{39}$$

Here, the expression in curly braces represents a 12-j symbol of the second kind (see Appendix D), $\langle n'_x\ell'_x s_{23}J_{23}T_{23}|V|n_xL_xs_{23}J_{23}T_{23}\rangle$ are two-body matrix elements of the nuclear interaction on the translational-invariant HO basis, and $\tilde{\gamma}'$ is an index associated with the HO channel states of Eq. (27) and identical to γ' except for the replacement of the quantum number ℓ'_x with L_x. In the present work, the Dirac's δ function in the y variables of Eq. (39) is approximated by an extended-size expansion in HO radial wave functions that goes well beyond the adopted HO model space ($N_{\rm ext}\gg N_{\rm max}$). The influence of such an approximation on the calculated binding energy of ^{6}He is small and is discussed in Sec. III.

Finally, with the exception of the terms proportional to the exchange part of the norm kernel, the action of the relative kinetic energy operator $\hat{T}_{\rm rel}$ and that of the eigenvalues $E^{I'_1T'_1}_{\alpha'}$ are both calculated in the full space.

III. APPLICATIONS TO ^{6}HE

It is well known that ^{6}He is the lightest Borromean nucleus [43,44], formed by an ^{4}He core and two halo neutrons. Owing to its small mass number and the fact that its constituents do not form bound subsystems, it is an ideal first candidate to be studied within the present approach.

The g.s. of this nucleus has been the subject of many investigations. Some of them are based on a three-body nonmicroscopic cluster formalism, representing it as a system of three inert particles [31,32,45–47]. This type of three-body method can lead to the appropriate asymptotic behavior of the wave function but does not allow for the exact treatment of the Pauli principle, which plays a fundamental role for light nuclei, and makes use of effective nucleon-nucleus potentials. There have also been *ab initio* six-body calculations focused on the g.s. of ^{6}He [48–52]. These are based on realistic Hamiltonians and fulfill the Pauli principle exactly. However, not taking explicitly into account the three-body cluster configuration of this nucleus leads to an incorrect description of the asymptotic properties of the system. Between these two approaches are microscopic calculations which take into account both the three-cluster configuration of the system and the internal structure of its constituents, giving a better description of the asymptotic behavior of the nuclear wave function while also preserving the Pauli principle [25,27–29,53,54]. Nevertheless, so far these types of calculations have been based on semirealistic interactions, often without spin-orbit force, and on a simplified description of the internal structure of the clusters.

In this work we present for the first time an *ab initio* calculation which not only uses realistic interactions but also takes into account the three-body configuration of this nucleus. In particular, we apply the formalism presented in Sec. II to study the g.s. of ^{6}He within a ^{4}He(g.s.) $+ n + n$ cluster basis. As stated in Sec. II E, the ^{4}He wave function is calculated within the NCSM formalism. In the present calculations, we describe the ^{4}He core only by its g.s. wave function, ignoring its excited states. The inclusion of excited states leads to big technical difficulties within the NCSM/RGM formalism because it increases notably the number of channels and the calculation becomes unbearable for current computational resources. However, this is a minor setback which, once the method is established as presented in this work, can be overcome by coupling the present three-cluster wave functions with NCSM eigenstates of the six-body system within the NCSMC [9,10] approach. For the time being, we estimate core polarization effects, by comparing the computed $J^\pi T = 0^+1$ ^{4}He(g.s.) $+$ $n + n$ g.s. energy with that obtained from an NCSM diagonalization of the six-body Hamiltonian. In both calculations, we use the same two-body interaction, namely, the SRG evolved [33,34] potential obtained from the chiral N^{3}LO NN interaction [35] with the evolution parameter $\Lambda = 1.5$ fm^{-1}.

A. ^{4}He and ^{6}He NCSM calculations

We performed NCSM calculations for ^{4}He that generated eigenstates needed as input for the subsequent three-body cluster NCSM/RGM investigations of ^{6}He. Further, we also calculated the g.s. energy of ^{6}He within the NCSM in order to make a comparison with the $^4\text{He} + n + n$ NCSM/RGM results. The computed ^{6}He g.s. energies for a range of HO frequencies and various basis sizes ($N_{\rm max}$ values) are presented in Fig. 2. As stated earlier, we are employing a soft SRG-evolved chiral N^{3}LO NN interaction with evolution parameter $\Lambda = 1.5$ fm^{-1}. We intentionally adopt such a soft interaction, for which our calculations reach convergence in the HO basis expansion already at the computationally accessible $N_{\rm max}\sim 12$. We can subsequently concentrate on the exploration of the validity of other approximations in the three-cluster NCSM/RGM formalism. We note that the same NN interaction was used in previous binary-cluster NCSM/RGM calculations of the d-^{4}He scattering [22] and d-^{3}H fusion [24]. The variational NCSM calculations converge rapidly and can

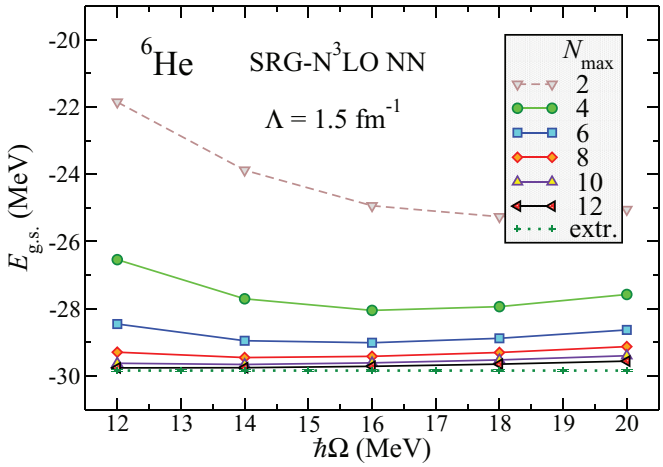

FIG. 2. (Color online) Convergence pattern of the binding energy of ^{6}He within the NCSM formalism.

be easily extrapolated to $N_{max} \to \infty$ using, e.g., an exponential function of the type $E(N_{max}) = E_\infty + ae^{-bN_{max}}$. As shown in Fig. 2, at $N_{max} = 12$ the dependence of the ^{6}He g.s. energy on the HO frequency is flat in the range of $\hbar\Omega \sim 12$–18 MeV. The variational minimum is close to $\hbar\Omega = 14$ MeV, which we then choose for the calculation of the ^{4}He eigenstates used as input for the $^4\text{He} + n + n$ NCSM/RGM investigations of the ^{6}He nucleus.

In Table I, the energy of ^{4}He and ^{6}He g.s.'s calculated with the NCSM formalism are shown (in MeV) in the second and last columns, respectively. To allow for a direct comparison with the NCSM/RGM calculation, results are listed as a function of the absolute HO model space size $N_{tot} = N_0 + N_{max}$, where N_0 is the number of oscillator quanta shared by the nucleons in their lowest configuration. For the ^{4}He nucleus $N_0 = 0$ and $N_{tot} = N_{max}$, but for the p-shell ^{6}He nucleus within the NCSM $N_{tot} = N_{max} + 2$. The extrapolated values of the NCSM calculation with their uncertainties and the experimental values [52] are also given. It can be observed that, with the present soft SRG interaction, the g.s. energy of ^{4}He is close to the experimental value, while the ^{6}He g.s. is overbound by about 0.5 MeV.

TABLE I. Computed NCSM ^{4}He, NCSM/RGM ^{6}He [as $^4\text{He(g.s.)} + n + n$] and NCSM ^{6}He g.s. energies (in MeV) as a function of the absolute HO model space size $N_{tot} = N_0 + N_{max}$, where N_0 is the number of oscillator quanta shared by the nucleons in their lowest configuration. For the ^{4}He nucleus and for the NCSM/RGM $^4\text{He} + n + n$ system, $N_0 = 0$ and $N_{max} = N_{tot}$. However, for the p-shell ^{6}He nucleus within the NCSM, $N_0 = 2$ and $N_{max} = N_{tot} - 2$. The last two rows show the extrapolated values for the calculations with their uncertainties and the experimental values.

N_{tot}	^{4}He NCSM	^{6}He NCSM/RGM	^{6}He NCSM
6	− 27.984	− 28.907	− 27.705
8	− 28.173	− 28.616	− 28.952
10	− 28.215	− 28.696	− 29.452
12	− 28.224	− 28.697	− 29.658
Extrapolation	− 28.230(5)	− 28.70(3)	− 29.84(4)
Experimental	− 28.296	− 29.268	

B. $^4\text{He} + n + n$ NCSM/RGM calculations

We performed calculations for the $^4\text{He} + n + n$ three-cluster system by using the NCSM/RGM formalism described in Sec. II. In this first application, we neglect core polarization effects and limit the description of ^{4}He to just the $I_1^{\pi_1} T_1 = 0^+0$ g.s. eigenstate in the NCSM/RGM coupled-channel equations. This is the only limitation of the model space introduced. None of the remaining quantum numbers contained in the cumulative index ν have any restriction other than those dictated by the model space size itself. In particular, we calculated Hamiltonian and norm kernels of Eqs. (6) and (7) for all possible J^π channels up to $J = 27$, the maximum value of the total angular momentum for our largest model space of $N_{max} = 13$, in which both the ℓ_x and the ℓ_y orbital angular momentum quantum numbers can vary from 0 to 13. Although, for the present paper we were exclusively interested in the 0^+ g.s. of ^{6}He, this was a necessary step to correctly extract the translational invariant matrix elements from our SD calculations through Eq. (31). Illustrative examples of the norm kernel are given in Sec. III B 1. The g.s. energy of ^{6}He is then obtained by solving the $^4\text{He} + n + n$ nonlocal hyper-radial equations (17) for the $J^\pi = 0^+$ channel with bound-state boundary conditions, as explained in Sec. II D. The dimension of the HH model space used for this part of the calculation is related to the maximum value of the hypermomentum K_{max}. Overall, the number of $\{\nu, K\}$ channels is very large (around 200 for the $J^\pi = 0^+$ state alone in our largest model space with $N_{max} = 13$ and $K_{max} = 28$). The dependence of our results for the ^{6}He g.s. with respect to both the HO and the HH expansions is discussed in Sec. III B 2.

1. Norm kernels

Particularly interesting are the elements of the exchange part of the norm kernel, $\mathcal{N}^{ex}_{\nu'\nu}(x', y', x, y)$, defined in Eq. (34), which give a measure of the influence of the Pauli exclusion principle. In Fig. 3, we present just a few of the most relevant examples. In addition, for visual purposes, we set the value of the primed coordinates x' and y' to 1 fm. In the present calculation, where the first cluster is given by the g.s. of ^{4}He, i.e., a $I_1^{\pi_1} T_1 = 0^+0$ state, and the second and third clusters are single nucleons, the various channels can be simply labeled by the spin and orbital angular momentum quantum numbers S, L, ℓ_x, and ℓ_y. As one would expect, for the largely s-shell ^{4}He core the antisymmetrization makes its largest contribution in the $S = L = \ell_x = \ell_y = 0$ channel of the 0^+ state, of which we show the diagonal "exchange" norm in Fig. 3(a). Large negative values of the exchange part of the norm kernel generally correspond to the presence of Pauli-forbidden components, in this case the $0\hbar\Omega$ component owing to the s-wave relative motion in both x and y coordinates. The norm is positive and much smaller in channels where the antisymmetrization plays a minor role, such as the $S = L = \ell_x = \ell_y = 1$ displayed in Fig. 3(c). The fairly symmetric appearance of these norm

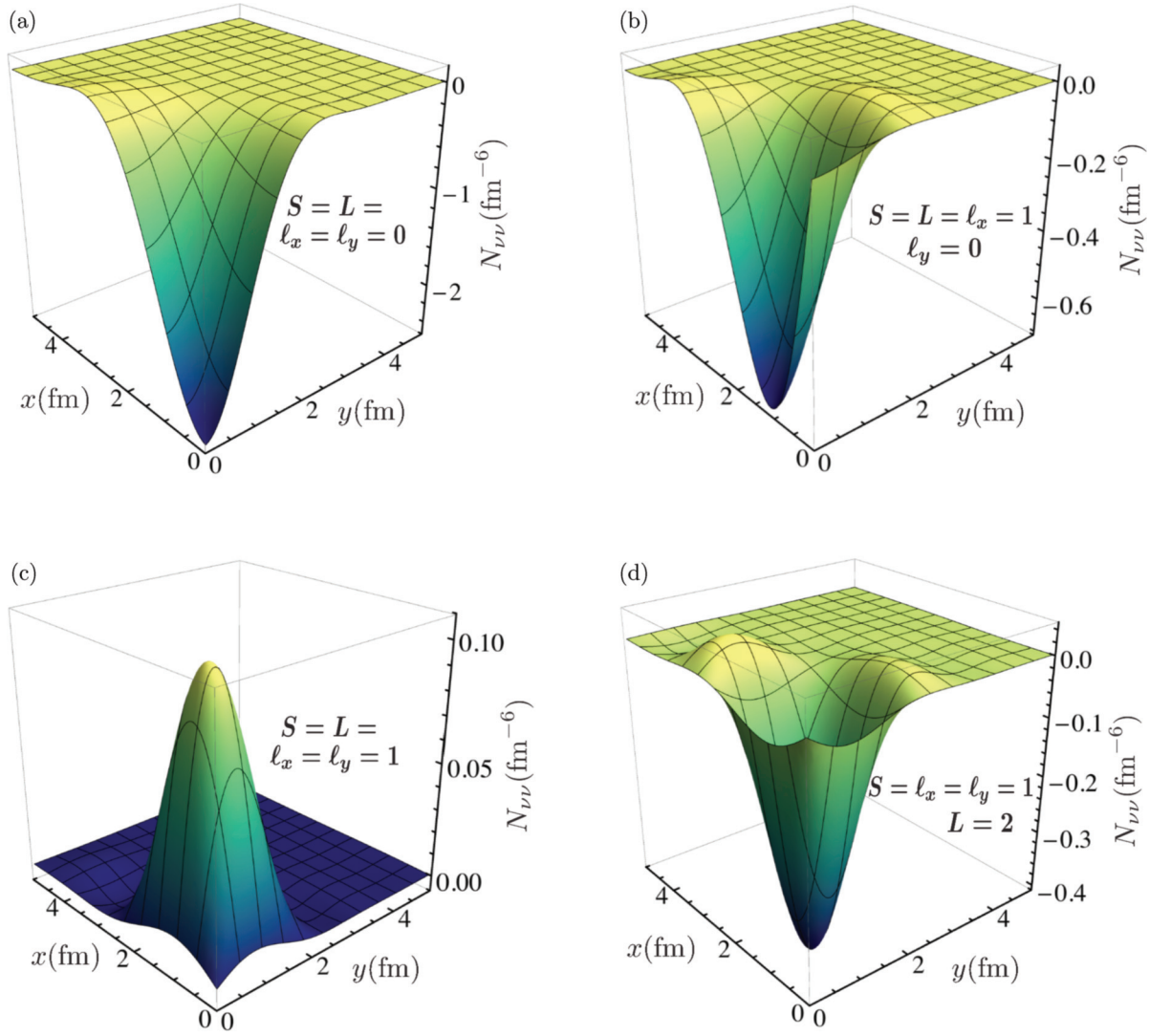

FIG. 3. (Color online) Diagonal elements of the exchange part of the norm kernel $\mathcal{N}^{\text{ex}}_{\nu\nu}(x', y', x, y)$ for the (a) $S = L = \ell_x = \ell_y = 0$, (b) $S = L = \ell_x = 1$, $\ell_y = 0$, (c) $S = L = \ell_x = \ell_y = 1$, and (d) $S = \ell_x = \ell_y = 1$, $L = 2$ partial waves. In each plot, the primed x' and y' coordinates are set to 1 fm.

kernels is caused by the equal value of the two orbital angular momenta ℓ_x and ℓ_y. However, the kernels are, in general, asymmetric in x, y (x', y') as is particularly evident in the $S = L = \ell_x = 1$, $\ell_y = 0$ case [Fig. 3(b)]. In this component, which appears in the 0^-, 1^-, and 2^- states, one can observe once again the repulsion owing to the Pauli principle in the y coordinate, while the p-wave motion forces the norm kernel to be null for $x = 0$ ($x' = 0$). Finally, in Fig. 3(d) we present the $S = \ell_x = \ell_y = 1$, $L = 2$ diagonal element of the 1^+, 2^+, and 3^+ exchange norm. In this channel, where one could naively expect a positive norm, we find a non-negligible negative contribution of the antisymmetrization, which suggests the presence of Pauli-forbidden components. These examples show that a correct treatment of the antisymmetrization not only is important to describe the g.s. of the ^{6}He nucleus, but also plays a role in important excited states such as the 1^- or 2^+ resonances.

2. ^{6}*He ground state*

To calculate the g.s. of ^{6}He, we first orthogonalize the NCSM/RGM equations, (5), as explained in Sec. II B and Appendix A. During this procedure the eigenvalues and eigenvectors of the norm kernel in the HO model space are calculated. For this $J^\pi T = 0^+1$ state, we observed the appearance of Pauli-forbidden norm eigenstates recognizable for their very small eigenvalues and negligible overlap with the physical g.s. eigenfunction. Spurious states can appear and admix with the low-lying physical eigenstates of the system if such Pauli-forbidden norm eigenstates are not eliminated. For the present calculation, we have removed all norm eigenstates with eigenvalues smaller than 0.1. In the $N_{\max} = 12$ model space, these amounted to a total of nine eigenstates with eigenvalues ranging from 0.58×10^{-3} to 0.62×10^{-1}. The unprecedented large number of $\{\nu n\}$ channels ($\sim$300) is likely responsible for the occurrence of such unphysical eigenstates

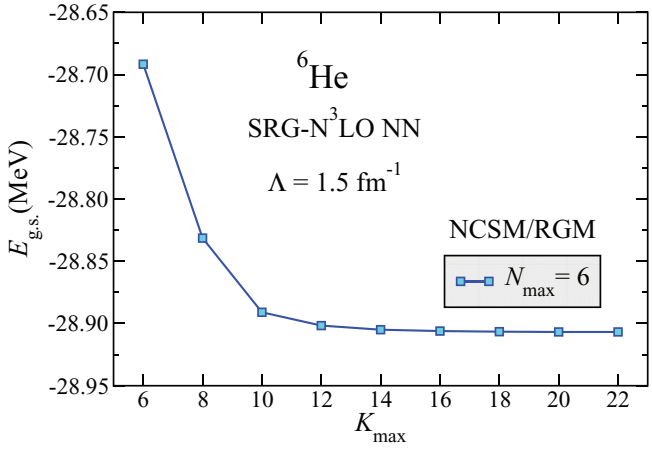

FIG. 4. (Color online) Dependence of the NCSM/RGM calculated ^{6}He g.s. energy at $N_{max} = 6$ as a function of the maximum value of the hypermomentum K_{max} used in the HH expansion. For these calculations we used a matching radius of $a = 20$ fm, $N = 30$ Lagrange mesh points, and an extended HO model space of $N_{ext} = 40$.

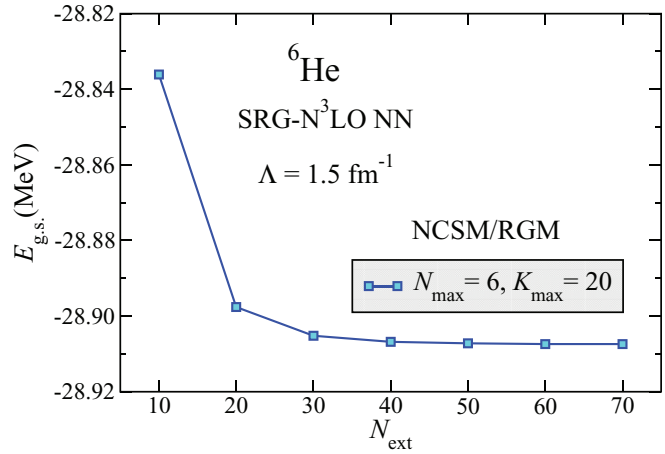

FIG. 5. (Color online) Dependence of the NCSM/RGM calculated ^{6}He g.s. energy at $N_{max} = 6$ as a function of the size of the extended HO model space N_{ext} used for the calculation of the interaction kernel of Eq. (39). For these calculations we used a hypermomentum of $K_{max} = 20$, a matching radius of $a = 20$ fm, and $N = 30$ ($N = 40$) Lagrange mesh points for $N_{ext} \leqslant 30$ ($N_{ext} > 30$).

of the norm, which had never been observed in our previous binary-cluster NCSM/RGM calculations.

We then expanded the orthogonalized NCSM/RGM equation, (10), in HH functions and solved the nonlocal hyper-radial equations (17) for the ^{4}He + n + n relative motion imposing bound-state boundary conditions, by using the R-matrix method on a Lagrange mesh from Sec. II D. We found a single bound state in the $J^\pi T = 0^+1$ channel and proceeded to study the behavior of our results at fixed N_{max} with respect to the remaining parameters of the calculation. Given the large scale of this computation, we performed this study at $N_{max} = 6$. The rate of convergence of the bound state with respect to the size of the adopted HH model space can be judged by examining Fig. 4, where we present a study of the calculated g.s. energy as a function of the maximum value of the hypermomentum K_{max}. The results start to stabilize around $K_{max} = 14$ and are fully converged already at $K_{max} = 20$. At a given N_{max}, the calculation is variational in K_{max}. Then we studied the stability of the g.s. energy with respect to the selection of the matching radius a, and we found that it was good as long as we chose values larger than 20 fm. The number N of mesh points required for a good convergence of the Lagrange expansion depends on the value of the matching radius. For $a = 20$ fm, about 30 mesh points are enough, while a larger number is needed if the matching radius is increased. The choice of the N value also depends somewhat on the size of the extended HO model space N_{ext} used to represent the Dirac's δ function in the y (y') coordinate (proportional to the distance between the centers of mass of the ^{4}He and the two neutrons) while calculating the interaction kernel of Eq. (39). Larger N_{ext} values correspond to a larger y range for this potential kernel, which is localized only in the x (x') coordinate. About 30 (40) mesh points are sufficient to reach convergence up to $N_{ext} = 30$ ($N_{ext} = 70$). The behavior of the g.s. energy as a function of N_{ext} is presented in Fig. 5. As shown, an extended HO basis size of at least $N_{ext} = 40$ is needed to accommodate the long range of this interaction kernel. Disregarding this effect by computing Eq. (39) within the adopted HO model space (i.e., with $N_{ext} = N_{max}$) leads to about 200 keV underbinding in the ^{6}He g.s. energy. Finally, a stable result for the integrations in the hyperangles α and α' of Eq. (18), which we perform numerically using a Chebyshev-Gauss quadrature (for Chebyshev polynomials of the second kind), was obtained with 20 mesh points. Based on this analysis and to ensure that convergence is reached, we adopted a matching radius of $a = 30$ fm with $N = 70$ mesh points, a hypermomentum $K_{max} = 28$, and an extended HO model space of $N_{ext} = 60$ for our larger N_{max} calculations (including the largest with $N_{max} = 12$) presented in the following. In Fig. 6 the main components of the radial part of the relative motion wave function $u_{Kv}^{J^\pi T}$ of the 0^+ g.s. of ^{6}He are shown for different values of the HO basis size N_{max} used for the expansions of the ^{4}He wave function and localized elements of the integration kernels. In the present calculation, each component is uniquely identified by the quantum numbers

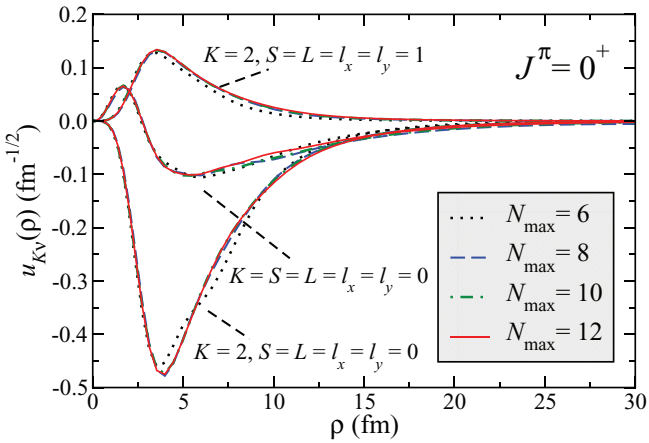

FIG. 6. (Color online) The three main components of the radial part of the ^{6}He g.s. wave functions $u_{Kv}(\rho)$ for $N_{max} = 6, 8, 10$, and 12.

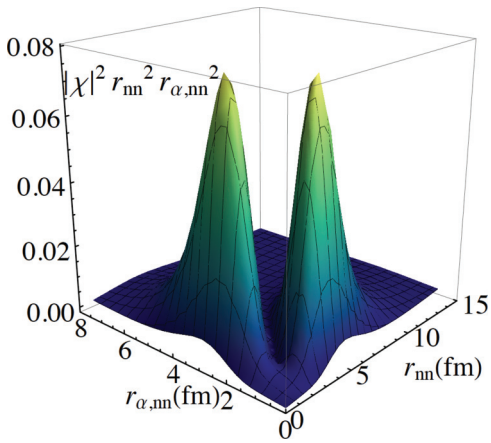

FIG. 7. (Color online) Probability distribution of the main component of the $^4\mathrm{He}+n+n$ relative motion wave function for the $J^\pi T = 0^+1$ ground state. The quantum numbers corresponding to this component are $S = L = \ell_x = \ell_y = 0$. Here $r_{nn} = \sqrt{2}\,\eta_{nn}$ and $r_{\alpha,nn} = \sqrt{3/4}\,\eta_{\alpha,nn}$ are, respectively, the distance between the two neutrons and the distance between the c.m. of ^{4}He and that of the two neutrons.

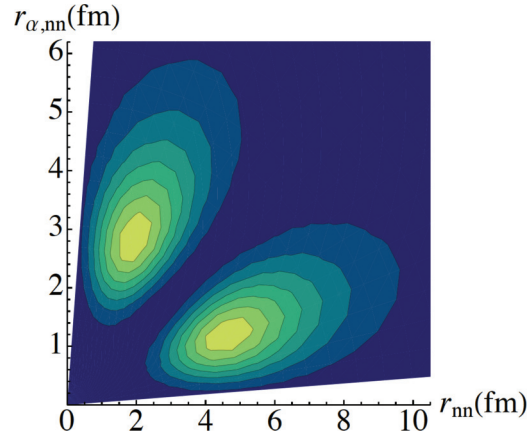

FIG. 8. (Color online) Contour diagram of the probability distribution plotted in Fig. 7.

shown in the figure. As can be seen, convergence is almost reached at $N_{\max} = 10$, and an $N_{\max} = 14$ calculation, which is currently out of computational reach, is not expected to substantially change the present results. This is confirmed also by the $N_{\max}$ dependence of the related g.s. energy, presented in the third column in Table I. Contrary to the NCSM, which gives rise to a Gaussian asymptotic behavior of the wave function owing to the use of expansions over six-body HO basis states, in the NCSM/RGM the $^4\mathrm{He(g.s.)}+n+n$ wave functions present the asymptotic behavior of Eq. (19), which is included by construction when using the R-matrix method. As shown in Fig. 6, the tails can extend up to about $\rho = 25$ fm. This feature will be of great importance when studying ^{6}He excited states, using scattering asymptotic conditions in the solution of the three-cluster equations.

Information about the three-cluster structure of the ^{6}He g.s. can be obtained by studying the probability distribution arising from the main component of the $^4\mathrm{He}+n+n$ relative motion wave function, presented as a surface plot in Fig. 7, and as a contour plot in Fig. 8. This component, characterized by the quantum numbers $S = L = \ell_x = \ell_y = 0$, presents the well-known [31] two-peak shape distribution. One peak corresponds to a "dineutron" configuration in which the neutrons are close together (about 2 fm apart) while the ^{4}He core is separated from their c.m. at a distance of about 3 fm, whereas the second peak, corresponding to the "cigar" configuration, represents an almost-linear structure in which the two neutrons are far from each other (about 5 fm apart) and the α particle lies almost in between them at $\sim$1 fm from their c.m. The position maxima of the two peaks can be more easily seen in the contour diagram in Fig. 8. The second most important contribution to the wave function comes from the component with quantum numbers $S = L = \ell_x = \ell_y = 1$, and the probability distribution arising from it is shown in Fig. 9. From the amplitude of the plot, it can be concluded that this component contributes very little to the complete wave function and does not significantly change the characteristic two-peak picture in Fig. 7.

The obtained ^{6}He g.s. energy (in units of MeV) for different sizes of the NCSM/RGM model space $N_{\max}$ are presented in the third column in Table I. The results of NCSM calculations of the ^{4}He and ^{6}He systems are shown in the second and last columns, respectively. At $N_{\max} = 12$, the NCSM/RGM calculation is basically converged within its uncertainty of about 30 keV, listed in the last row. The effect of the exclusion of the spurious eigenstates of the norm, discussed at the beginning of this section, is included in this uncertainty. Unlike the NCSM case, the present NCSM/RGM calculations are not variational in the HO model space size, as at each $N_{\max}$ value the three-cluster basis contains a different ^{4}He eigenstate. It can be observed that in the NCSM/RGM the ^{6}He g.s. is underbound. In particular, the energy is about 1 MeV higher than the one obtained within the NCSM. This difference is caused by excitations of the ^{4}He core, which, for technical reasons, are included only in the NCSM calculation at present. In this sense, the difference between the two calculations provides a measure of core polarization effects in ^{6}He.

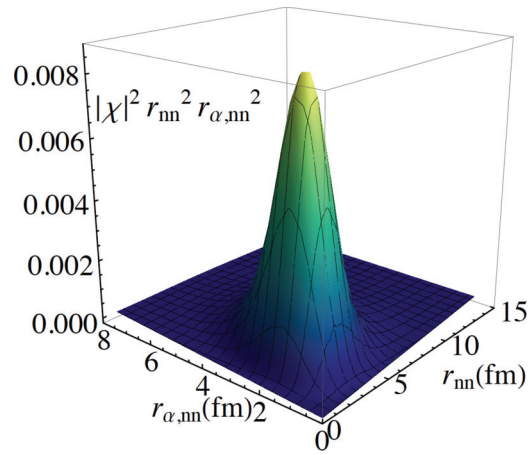

FIG. 9. (Color online) Same as Fig. 7, but for the second most important component. The quantum numbers corresponding to this component are $S = L = \ell_x = \ell_y = 1$.

IV. CONCLUSIONS

In this work, we have extended the NCSM/RGM method [19,20] to the treatment of three-cluster dynamics. This new feature permits us to study a new range of systems that present three-body configurations. In particular, in this work we show that it can be used to study the structure of two-neutron halo nuclei such as ^{6}He and, contrary to other *ab initio* methods such as the NCSM, to obtain the appropriate asymptotic behavior of its wave functions. Moreover, the present formalism combined with the appropriate scattering boundary conditions gives access to the *ab initio* study of resonant states of two-neutron halo nuclei (such as the excited states of ^{6}He) as well as to scattering problems involving channels with three fragments. Three-cluster NCSM/RGM $^4\mathrm{He}+n+n$ scattering calculations with the aim of studying ^{6}He low-lying resonances are currently under way and will be reported in a subsequent paper.

For the present study of ^{6}He within the $^4\mathrm{He}+n+n$ cluster basis, we used only the g.s. wave function to describe the ^{4}He core. This leads to an underbinding of the ^{6}He g.s. owing to the missing treatment of core polarization. The difference with respect to the energy obtained from a diagonalization of the Hamiltonian in an NCSM six-body model space indicates that, with the present soft NN interaction, core-polarization effects amount to less than 5% of the binding. This is, however, a much larger effect if one considers that it represents about two-thirds of the separation energy with respect to the $^4\mathrm{He}+n+n$ threshold. The inclusion of excited states of ^{4}He would significantly increase the number of channels in the calculation, making it computationally unbearable. Core polarization effects can be more efficiently taken into account by coupling the present three-cluster wave functions with six-body NCSM eigenstates within the NCSMC framework. While the results of this approach will be presented in a forthcoming publication, the main difficulty of such a calculation resides in obtaining the three-cluster NCSM/RGM wave functions and has been addressed in the present work.

ACKNOWLEDGMENTS

We thank G. Hupin for many useful discussions. Computing support for this work came from the LLNL institutional Computing Grand Challenge program and from an INCITE Award on the Titan supercomputer of the Oak Ridge Leadership Computing Facility (OLCF) at ORNL. The work was prepared in part by LLNL under Contract No. DE-AC52-07NA27344. Support from the U.S. DOE/SC/NP (Work Proposal No. SCW1158) and NSERC Grant No. 401945-2011 is acknowledged. TRIUMF receives funding via a contribution through the Canadian National Research Council.

APPENDIX A: ORTHOGONALIZATION

The appearance of the norm kernel $\mathcal{N}^{J^\pi T}_{\nu'\nu}(x',y',x,y)$ in Eq. (5) reflects the fact that the many-body wave function $\Psi^{J^\pi T}$ is expanded in terms of a nonorthogonal basis. Therefore, Eq. (5) does not represent a system of multichannel Schrödinger equations, and $G^{J^\pi T}_\nu(x,y)$ do not represent Schrödinger wave functions. However, one can solve the equivalent set of orthogonalized equations introduced in Eq. (10), where

$$\begin{aligned}\bar{\mathcal{H}}^{J^\pi T}_{\nu'\nu}(x',y',x,y) &= \sum_{\tilde\nu'}\iint d\tilde x' d\tilde y' \tilde x'^2\tilde y'^2 \sum_{\tilde\nu}\iint d\tilde x\, d\tilde y\, \tilde x^2\tilde y^2 \\ &\times \mathcal{N}^{-1/2}_{\nu'\tilde\nu'}(x',y',\tilde x',\tilde y')\mathcal{H}^{J^\pi T}_{\tilde\nu'\tilde\nu}(\tilde x',\tilde y',\tilde x,\tilde y)\mathcal{N}^{-1/2}_{\tilde\nu\nu}(\tilde x,\tilde y,x,y)\end{aligned} \tag{A1}$$

is the orthogonalized Hamiltonian kernel and the Schrödinger wave functions $\chi^{J^\pi T}_\nu(x,y)$ are the new unknowns of the problem, related to $G^{J^\pi T}_\nu(x,y)$ through

$$\begin{aligned}G^{J^\pi T}_\nu(x,y) &= \sum_{\tilde\nu}\iint d\tilde x\, d\tilde y\, \tilde x^2\,\tilde y^2 \mathcal{N}^{-\frac{1}{2}}_{\nu\tilde\nu}(x,y,\tilde x,\tilde y)\,\chi^{J^\pi T}_{\tilde\nu}(\tilde x,\tilde y).\end{aligned} \tag{A2}$$

Here, $\mathcal{N}^{1/2}_{\nu'\nu}(x',y',x,y)$ and $\mathcal{N}^{-1/2}_{\nu'\nu}(x',y',x,y)$ represent the square root and the inverse-square root of the norm kernel, respectively, which are obtained as follows. First, we add and subtract from the norm kernel the identity in the HO model space:

$$\begin{aligned}\mathcal{N}^{J^\pi T}_{\nu'\nu}(x',y',x,y) &= \delta_{\nu\nu'}\left[\frac{\delta(x'-x)}{x'x}\frac{\delta(y'-y)}{y'y}\right. \\ &\left. - \sum_{n_x n_y} R_{n_x\ell_x}(x')R_{n_x\ell_x}(x)R_{n_y\ell_y}(y')R_{n_y\ell_y}(y)\right] \\ &+ \Lambda^{J^\pi T}_{\nu'\nu}(x',y',x,y).\end{aligned} \tag{A3}$$

The norm kernel within the truncated model space, $\Lambda^{J^\pi T}_{\nu'\nu}(x',y',x,y)$, is obtained by using expansion (26) with the matrix elements on the HO Jacobi-channel states of Eq. (27) given by

$$\Lambda^{J^\pi T}_{\gamma' n'_x n'_y,\gamma n_x n_y} = \delta_{n_x,n'_x}\delta_{n_y,n'_y}\delta_{\gamma,\gamma'} + \mathcal{N}^{\mathrm{ex}}_{\gamma' n'_x n'_y,\gamma n_x n_y} \tag{A4}$$

and $\mathcal{N}^{\mathrm{ex}}_{\gamma' n'_x n'_y,\gamma n_x n_y}$ as defined in Eq. (35). Then the square and the inverse-square root of the full-space norm are obtained by (i) finding the eigenvalues λ_Γ and eigenvectors $|\varphi^{J^\pi T}_\Gamma\rangle$ of matrix $\Lambda^{J^\pi T}$ of Eq. (A4); (ii) calculating

$$\Lambda^{\pm1/2}_{\gamma' n'_x n'_y,\gamma. n_x n_y} = \sum_\Gamma \left\langle \Phi^{J^\pi T}_{\gamma' n'_x n'_y}\middle|\varphi^{J^\pi T}_\Gamma\right\rangle \lambda^{\pm1/2}_\Gamma \left\langle\varphi^{J^\pi T}_\Gamma\middle|\Phi^{J^\pi T}_{\gamma n_x n_y}\right\rangle \tag{A5}$$

and the corresponding integration kernels through expansion (26), and, finally, (iii) replacing the model-space norm $\Lambda^{J^\pi T}_{\nu'\nu}(x',y',x,y)$ in Eq. (A3) with $\Lambda^{\pm1/2}_{\nu'\nu}(x',y',x,y)$; that is,

$$\begin{aligned}\mathcal{N}^{\pm1/2}_{\nu'\nu}(x',y',x,y) &= \delta_{\nu\nu'}\left[\frac{\delta(x'-x)}{x'x}\frac{\delta(y'-y)}{y'y}\right. \\ &\left. - \sum_{n_x n_y} R_{n_x\ell_x}(x')R_{n_x\ell_x}(x)R_{n_y\ell_y}(y')R_{n_y\ell_y}(y)\right] \\ &+ \Lambda^{\pm1/2}_{\nu'\nu}(x',y',x,y).\end{aligned} \tag{A6}$$

For the inverse operation to be permissible in Eq. (A5) one has to exclude the subspace of (fully) Pauli-forbidden states for which $\lambda_\Gamma = 0$.

APPENDIX B: HH CHANNEL BASIS

Using the Dirac δ properties and completeness relation of the set of $\phi_K^{\ell_x \ell_y}$ functions, we have

$$\frac{\delta(x-\eta_{23})}{x\,\eta_{23}}\frac{\delta(y-\eta_{1,23})}{y\,\eta_{1,23}} = \frac{\delta(\rho-\rho_\eta)}{\rho^{5/2}\,\rho_\eta^{5/2}}\frac{\delta(\alpha-\alpha_\eta)}{\sin\alpha\cos\alpha\,\sin\alpha_\eta\cos\alpha_\eta} = \frac{\delta(\rho-\rho_\eta)}{\rho^{5/2}\,\rho_\eta^{5/2}}\sum_K \phi_K^{\ell_x,\ell_y}(\alpha_\eta)\phi_K^{*\ell_x,\ell_y}(\alpha); \tag{B1, B2}$$

then the three-cluster channel states of Eq. (2) can be written as

$$\left|\Phi_{\nu xy}^{J^\pi T}\right\rangle = \sum_K \phi_K^{*\ell_x,\ell_y}(\alpha)\left|\Phi_{\nu K\rho}^{J^\pi T}\right\rangle, \tag{B3}$$

where $|\Phi_{\nu K\rho}^{J^\pi T}\rangle$ are the channel states in the HH basis

$$\left|\Phi_{\nu K\rho}^{J^\pi T}\right\rangle = \left[\left(\left|A-a_{23}\alpha_1 I_1^{\pi_1}T_1\right\rangle\left(\left|a_2\,\alpha_2 I_2^{\pi_2}T_2\right\rangle\left|a_3\,\alpha_3 I_3^{\pi_3}T_3\right\rangle\right)^{(s_{23}T_{23})}\right)^{(ST)}\mathcal{Y}_L^{K\ell_x\ell_y}(\Omega_\eta)\right]^{(J^\pi T)}\frac{\delta(\rho-\rho_\eta)}{\rho^{5/2}\,\rho_\eta^{5/2}}, \tag{B4}$$

with $\Omega_\eta = \{\alpha_\eta, \hat{\eta}_{23}, \hat{\eta}_{1,23}\}$ and $\mathcal{Y}_L^{K\ell_x\ell_y}(\Omega_\eta)$ the HH basis elements defined in Eq. (14). At the same time, inserting this expansion in Eq. (1), changing from x and y to the HH coordinates ρ and α, and integrating over the hyperangle α, one can demonstrate that the many-body wave function is also given by

$$\left|\Psi^{J^\pi T}\right\rangle = \sum_{\nu K}\int d\rho\,\rho^5\frac{g_{K\nu}^{J^\pi T}(\rho)}{\rho^{5/2}}\hat{\mathcal{A}}_\nu\left|\Phi_{\nu K\rho}^{J^\pi T}\right\rangle, \tag{B5}$$

where the hyper-radial functions $g_{K\nu}^{J^\pi T}(\rho)$ are obtained from the projection of the variational amplitudes $G_\nu^{J^\pi T}(\rho\sin\alpha, \rho\cos\alpha)$ over the functions $\phi_K^{\ell_x,\ell_y}(\alpha)$:

$$\frac{g_{K\nu}^{J^\pi T}(\rho)}{\rho^{5/2}} = \int d\alpha\,\sin^2\alpha\cos^2\alpha \times \phi_K^{*\ell_x,\ell_y}(\alpha)\,G_\nu^{J^\pi T}(\rho\sin\alpha, \rho\cos\alpha). \tag{B6}$$

APPENDIX C: LAGRANGE BASIS

We use a Lagrange basis which is a set of N functions $f_n(x)$ (see [42] and references therein), given by

$$f_n(x) = (-1)^n a^{-1/2}\sqrt{\frac{1-x_n}{x_n}}\frac{x\,P_N(2x/a-1)}{x-ax_n}, \tag{C1}$$

where $P_N(x)$ are Legendre polynomials, and x_n satisfy

$$P_N(2x_n-1) = 0. \tag{C2}$$

The Lagrange mesh associated with this basis consists in N points ax_n on the interval $[0, a]$ and satisfies the Lagrange conditions

$$f_{n'}(ax_n) = \frac{1}{\sqrt{a\lambda_n}}\delta_{nn'}, \tag{C3}$$

where the coefficients λ_n are the weights corresponding to a Gauss-Legendre quadrature approximation for the [0, 1] interval; i.e.,

$$\int_0^1 g(x)dx \sim \sum_{n=1}^N \lambda_n g(x_n). \tag{C4}$$

Using the Lagrange conditions of Eq. (C3), it is straightforward to see that within the Gauss approximation the Lagrange functions are orthogonal; i.e.,

$$\int_0^a f_n(x)f_{n'}(x)dx \sim \delta_{nn'}. \tag{C5}$$

APPENDIX D: 12-j SYMBOL DEFINITION

The 12-j symbol of the second kind [55] is defined by

$$\begin{Bmatrix} - & a_2 & a_3 & a_4 \\ b_1 & - & b_3 & b_4 \\ c_1 & c_2 & - & c_4 \\ d_1 & d_2 & d_3 & - \end{Bmatrix} = (-1)^{b_3-a_4-d_1+c_2}\sum_x (2x+1)\begin{Bmatrix} a_3 & b_4 & x \\ b_1 & d_3 & b_3 \end{Bmatrix}\begin{Bmatrix} a_3 & b_4 & x \\ c_4 & a_2 & a_4 \end{Bmatrix}\begin{Bmatrix} b_1 & d_3 & x \\ d_2 & c_1 & d_1 \end{Bmatrix}\begin{Bmatrix} c_4 & a_2 & x \\ d_2 & c_1 & c_2 \end{Bmatrix}$$

$$= (-1)^{b_3-a_4-d_1+c_2}\sum_x (2x+1)\begin{Bmatrix} a_3 & b_3 & d_3 \\ a_4 & b_4 & c_4 \\ a_2 & b_1 & x \end{Bmatrix}\begin{Bmatrix} d_2 & d_1 & d_3 \\ c_2 & c_1 & c_4 \\ a_2 & b_1 & x \end{Bmatrix}. \tag{D1}$$

[1] H. Kamada, A. Nogga, W. Glöckle, E. Hiyama, M. Kamimura, K. Varga, Y. Suzuki, M. Viviani, A. Kievsky, S. Rosati, J. Carlson, S. C. Pieper, R. B. Wiringa, P. Navrátil, B. R. Barrett, N. Barnea, W. Leidemann, and G. Orlandini, Phys. Rev. C **64**, 044001 (2001).

[2] M. Viviani, A. Deltuva, R. Lazauskas, J. Carbonell, A. C. Fonseca, A. Kievsky, L. E. Marcucci, and S. Rosati, Phys. Rev. C **84**, 054010 (2011).

[3] K. M. Nollett, S. C. Pieper, R. B. Wiringa, J. Carlson, and G. M. Hale, Phys. Rev. Lett. **99**, 022502 (2007).

[4] K. M. Nollett and R. B. Wiringa, Phys. Rev. C **83**, 041001 (2011).

[5] K. M. Nollett, Phys. Rev. C **86**, 044330 (2012).

[6] G. Hagen, D. J. Dean, M. Hjorth-Jensen, and T. Papenbrock, Phys. Lett. B **656**, 169 (2007).

[7] G. Hagen, T. Papenbrock, and M. Hjorth-Jensen, Phys. Rev. Lett. **104**, 182501 (2010).

[8] G. Hagen and N. Michel, Phys. Rev. C **86**, 021602 (2012).

[9] S. Baroni, P. Navrátil, and S. Quaglioni, Phys. Rev. Lett. **110**, 022505 (2013).

[10] S. Baroni, P. Navrátil, and S. Quaglioni, Phys. Rev. C **87**, 034326 (2013).

[11] K. Wildermuth and Y. C. Tang, *A Unified Theory of the Nucleus* (Vieweg, Braunschweig, 1977).

[12] Y. Tang, M. LeMere, and D. Thompsom, Phys. Rep. **47**, 167 (1978).

[13] T. Fliessbach and H. Walliser, Nucl. Phys. A **377**, 84 (1982).

[14] K. Langanke and H. Friedrich, *Advances in Nuclear Physics* (Plenum Press, New York, 1986).

[15] R. Lovas, R. Liotta, A. Insolia, K. Varga, and D. Delion, Phys. Rep. **294**, 265 (1998).

[16] H. M. Hofmann and G. M. Hale, Phys. Rev. C **77**, 044002 (2008).

[17] P. Navrátil, J. P. Vary, and B. R. Barrett, Phys. Rev. Lett. **84**, 5728 (2000).

[18] P. Navrátil, J. P. Vary, and B. R. Barrett, Phys. Rev. C **62**, 054311 (2000).

[19] S. Quaglioni and P. Navrátil, Phys. Rev. Lett. **101**, 092501 (2008).

[20] S. Quaglioni and P. Navrátil, Phys. Rev. C **79**, 044606 (2009).

[21] P. Navrátil, R. Roth, and S. Quaglioni, Phys. Rev. C **82**, 034609 (2010).

[22] P. Navrátil and S. Quaglioni, Phys. Rev. C **83**, 044609 (2011).

[23] P. Navrátil, R. Roth, and S. Quaglioni, Phys. Lett. B **704**, 379 (2011).

[24] P. Navrátil and S. Quaglioni, Phys. Rev. Lett. **108**, 042503 (2012).

[25] G. F. Filippov, K. Kato, and S. V. Korennov, Prog. Theor. Phys. **96**, 575 (1996).

[26] V. Vasilevsky, A. V. Nesterov, F. Arickx, and J. Broeckhove, Phys. Rev. C **63**, 034606 (2001).

[27] V. Vasilevsky, A. V. Nesterov, F. Arickx, and J. Broeckhove, Phys. Rev. C **63**, 034607 (2001).

[28] S. Korennov and P. Descouvemont, Nucl. Phys. A **740**, 249 (2004).

[29] A. Damman and P. Descouvemont, Phys. Rev. C **80**, 044310 (2009).

[30] V. Vasilevsky, F. Arickx, W. Vanroose, and J. Broeckhove, Phys. Rev. C **85**, 034318 (2012).

[31] P. Descouvemont, C. Daniel, and D. Baye, Phys. Rev. C **67**, 044309 (2003).

[32] P. Descouvemont, E. Tursunov, and D. Baye, Nucl. Phys. A **765**, 370 (2006).

[33] S. K. Bogner, R. J. Furnstahl, and R. J. Perry, Phys. Rev. C **75**, 061001 (2007).

[34] R. Roth, S. Reinhardt, and H. Hergert, Phys. Rev. C **77**, 064003 (2008).

[35] D. R. Entem and R. Machleidt, Phys. Rev. C **68**, 041001 (2003).

[36] A. Kievsky, S. Rosati, M. Viviani, L. E. Marcucci, and L. Girlanda, J. Phys. G: Nucl. Part. Phys. **35**, 063101 (2008).

[37] M. Fabre de la Ripelle, Ann. Phys. **147**, 281 (1983).

[38] P. Descouvemont and D. Baye, Rep. Prog. Phys. **73**, 036301 (2010).

[39] D. Baye, J. Goldbeter, and J.-M. Sparenberg, Phys. Rev. A **65**, 052710 (2002).

[40] D. Baye, M. Hesse, J.-M. Sparenberg, and M. Vincke, J. Phys. B: At. Mol. Opt. Phys. **31**, 3439 (1998).

[41] M. Hesse, J. Roland, and D. Baye, Nucl. Phys. A **709**, 184 (2002).

[42] M. Hesse, J.-M. Sparenberg, F. Van Raemdonck, and D. Baye, Nucl. Phys. A **640**, 37 (1998).

[43] I. Tanihata, J. Phys. G **22**, 157 (1996).

[44] I. Tanihata, H. Hamagaki, O. Hashimoto, Y. Shida, N. Yoshikawa, K. Sugimoto, O. Yamakawa, T. Kobayashi, and N. Takahashi, Phys. Rev. Lett. **55**, 2676 (1985).

[45] V. I. Kukulin, V. M. Krasnopol'sky, V. T. Voronchev, and P. B. Sazonov, Nucl. Phys. A **453**, 365 (1986).

[46] M. Zhukov, B. Danilin, D. Fedorov, J. Bang, I. Thompson, and J. Vaagen, Phys. Rep. **231**, 151 (1993).

[47] P. Descouvemont, E. Pinilla, and D. Baye, Prog. Theor. Phys. (Suppl.) **196**, 1 (2012).

[48] S. Bacca, A. Schwenk, G. Hagen, and T. Papenbrock, Eur. Phys. J. A **42**, 553 (2009).

[49] I. Brida and F. M. Nunes, Nucl. Phys. A **847**, 1 (2010).

[50] P. Navrátil and W. E. Ormand, Phys. Rev. C **68**, 034305 (2003).

[51] S. Pieper and R. Wiringa, Annu. Rev. Nucl. Part. Sci. **51**, 53 (2001).

[52] M. Brodeur, T. Brunner, C. Champagne, S. Ettenauer, M. Smith *et al.*, Phys. Rev. Lett. **108**, 052504 (2012).

[53] K. Varga, Y. Suzuki, and Y. Ohbayasi, Phys. Rev. C **50**, 189 (1994).

[54] K. Arai, Y. Suzuki, and R. G. Lovas, Phys. Rev. C **59**, 1432 (1999).

[55] D. Varshalovich, A. Moskalev, and V. Khersonskiĭ, *Quantum Theory of Angular Momentum* (World Scientific, Singapore, 1988).